Analytical solution and Bayesian inference for interference pumping tests in fractal dual-porosity media

Mohamed Hayek, Anis Younes, Jabran Zouali, Noura Fajraoui, Marwan Fahs

Analytical solution and Bayesian inference for interference pumping tests in fractal dual-porosity media

Mohamed Hayek[1], Anis Younes[*,2,3,4], Jabran Zouali[2], Noura Fajraoui[5], Marwan Fahs[2]

[1]AF-Consult, Groundwater Protection and Waste Disposal, Täfernstrasse 26, CH-5405 Baden, Switzerland
[2]LHyGES, Université de Strasbourg/EOST, CNRS, 1 rue Blessig, 67084 Strasbourg, France
[3] IRD UMR LISAH, F-92761 Montpellier, France
[4] LMHE, Ecole Nationale d'Ingénieurs de Tunis, Tunisie
[5] Chair of Risk, Safety and Uncertainty Quantification, ETH Zurich, Switzerland

Submitted to *Computational Geosciences*

* *Contact person: younes@unistra.fr*

Abstract

A new analytical solution is developed for interference hydraulic pumping tests in fractured porous media using the dual-porosity concept. Heterogeneous fractured reservoirs are considered with hydrodynamic parameters assumed to follow power-law functions in radial distance. The developed analytical solution is verified by comparison against a finite volume numerical solution. The comparison shows that the numerical solution converges toward the analytical one when the size of the time step decreases. The applicability of the fractal dual-porosity model is then assessed by investigating the identifiability of the parameters from a synthetic interference pumping test with a set of noisy data using Bayesian parameter inference. The results show that if the storage coefficient in the matrix is fixed, the rest of the parameters can be appropriately inferred, otherwise, the identification of the parameters is faced with convergence problems because of equifinality issues.

Keywords: Fractured porous media, interference pumping test, dual-porosity, fractal media, Bayesian inversion.

1 INTRODUCTION

Simulation of interference pumping tests in porous media allows testing different prospective exploitation scenarios at low costs. These tests consist in pumping a well at a controlled flow rate and measuring the water level response (drawdown) in one or more surrounding observation wells. Pumping tests in fractured porous media have been discussed by several authors (see [1-8], among others). Fractured media are often addressed using the dual-porosity model suggested by Barenblatt *et al.* [9]. The main idea of this model is to consider two overlapping continua: (*i*) the fractures which carry the major part of water to the pumping well and (*ii*) the low permeability rock matrix which feeds fluid to the fractures. At each point of the domain, water flow between the fractures and matrix are coupled via a linear exchange term proportional to the difference in hydraulic head between the two continua. As stated by De Smedt [8], the simulation of interference pumping tests is often based on numerical models which cannot insure full control of numerical accuracy [10]. Therefore, analytical solutions are highly sought-after because (*i*) they provide valuable insights into fundamental physics, as they are free of numerical errors and (*ii*), although limited to simplified situations; they allow validation of more complex numerical codes.

In the context of interference pumping tests in fractured porous media, an analytical solution has been developed for homogenous aquifers by De Smedt [8]. Furthermore, Delay et al. [7] developed a numerical solution using the dual-medium approach to describe radial convergent flow in heterogeneous fractal media where power laws in space are used for the hydrodynamic parameters. As a consequence, parameter values decrease with the distance between the pumped well and the observed ones. This type of scaling laws inherits from theoretical works on fractals [11] and has been used by several authors for single porous media ([12-15], among others). Hence, the main objective of this paper is to develop, for the first time, an analytical solution for the mathematical model describing interference pumping tests in heterogeneous

fractal dual media. Applicability of the model is then assessed by investigating identifiability of the different parameters from a synthetic pumping test with a set of noisy data using Statistical Calibration (SC) [16]. The latter means refining the prior distribution of uncertain parameters based on matching simulation outputs with data [17]. In this work, the SC is performed with the DREAM$_{(ZS)}$ software [16] based on the Markov Chain Monte Carlo process (MCMC). DREAM$_{(ZS)}$ computes multiple sub-chains in parallel to thoroughly explore the parameter space. Taking the last 25% of individuals of the MCMC (when the chains have converged) yields multiple sets of parameters that adequately fit the model onto observations. These sets can then be used to estimate the updated parameter distributions and therefore the best estimates of the parameters and the associate confidence intervals.

2 MATHEMATICAL MODEL

We assume a horizontal, isotropic, confined and infinite aquifer with a uniform thickness. The pumping well only draws water from the fractures, has a constant rate and fully penetrates the aquifer. Using the dual-porosity concept, the flow in fractured porous media can be described by the following equations [18, 19]:

$$S_f \frac{\partial h_f}{\partial t} = \nabla.\left(K_f \nabla h_f\right) + \alpha\left(h_m - h_f\right) \quad (1)$$

$$S_m \frac{\partial h_m}{\partial t} = \alpha\left(h_f - h_m\right) \quad (2)$$

where indexes m and f refer to the matrix and fracture continua, respectively, $S\left[L^{-1}\right]$ is the specific storage, $h[L]$ is the hydraulic head, $K_f\left[LT^{-1}\right]$ is the hydraulic conductivity of the fractures, $\alpha\left[L^{-1}T^{-1}\right]$ is the exchange rate coefficient between the fractures and the matrix. Following Warren and Root [18], equation (2) assumes pseudo-steady flow in the matrix con-

tinuum (term K_m is removed). Assuming radial symmetry, equations (1) and (2) can be formulated as:

$$S_f(r)\frac{\partial h_f(r,t)}{\partial t}=\frac{1}{r}\frac{\partial}{\partial r}\left[rK_f(r)\frac{\partial h_f(r,t)}{\partial r}\right]+\alpha(r)\left[h_m(r,t)-h_f(r,t)\right] \tag{3}$$

$$S_m(r)\frac{\partial h_m(r,t)}{\partial t}=\alpha(r)\left[h_f(r,t)-h_m(r,t)\right] \tag{4}$$

where $r[L]$ is the radial coordinate with the center of the pumping well as origin.

The drawdown in an observation well intercepting the fractures can be expressed as follows

$$S_f(r)\frac{\partial H_f(r,t)}{\partial t}=\frac{1}{r}\frac{\partial}{\partial r}\left(rK_f(r)\frac{\partial H_f(r,t)}{\partial r}\right)+\alpha(r)\left[H_m(r,t)-H_f(r,t)\right] \tag{5}$$

$$S_m(r)\frac{\partial H_m(r,t)}{\partial t}=\alpha(r)\left[H_f(r,t)-H_m(r,t)\right] \tag{6}$$

where $H_f=h_0-h_f$ and $H_m=h_0-h_m$ are respectively the drawdown in the fracture and in the rock matrix. Initially, a uniform hydraulic head (h_0) is assumed in both the fracture and matrix continua. Therefore, the drawdowns satisfy the following initial conditions:

$$H_f(r,0)=H_m(r,0)=0 \tag{7}$$

Far away from the pumping well, the drawdowns are assumed to be zero

$$\lim_{r\to\infty}H_f(r,t)=\lim_{r\to\infty}H_m(r,t)=0 \tag{8}$$

The limit where the radius approaches zero corresponds to the well withdrawal rate

$$\lim_{r\to 0}\left[-2\pi rBK_f(r)\frac{\partial H_f(r,t)}{\partial r}\right]=Q_0,\quad t>0 \tag{9}$$

where B is the thickness of the aquifer and Q_0 is the pumping flow rate.

In the sequel, we limit our investigation for the semi-analytical solution of equations (5-9) to the case of a confined reservoir of a fractal structure with a single well in an unbounded me-

dium as described in [7, 12]. Note that more complex fractal approaches have been developed in the case of many wells with variable rates [20] and by considering transient flow from block to fissure and skin between the fissure and the block [21].

In this work, following Delay *et al.* [7], we consider dual porosity media in which the hydrodynamic parameters are power-law functions in space (decreasing functions of the radial distance r between the pumping well and the observed one). Moreover, for sake of simplicity, we assume the same functions for the exchange rate coefficient α and for the storage coefficients S_f and S_m. Hence, the values of the hydraulic parameters vary with respect to radial distance according to the following power-law functions:

$$\begin{aligned} K_f(r) &= K_{f_0} r^{-a}; \quad S_f(r) = S_{f_0} r^{-b} \\ S_m(r) &= S_{m_0} r^{-b}; \quad \alpha(r) = \alpha_0 r^{-b} \end{aligned} \tag{10}$$

where the power-law exponents a and b are assumed to be positive.

3 ANALYTICAL SOLUTION

3.1 Analytical solution in the Laplace domain

In this section, we follow the strategy developed by De Smedt [8] to derive the analytical solution of the system formed by equations (5)-(10). The solution is derived using the Laplace transform technique with respect to time variable t. The Laplace transform of a time-dependent function y is

$$\bar{y}(p) = L\left[y(t); t \to p\right] = \int_0^\infty y(t) e^{-pt} \mathrm{d}t \tag{11}$$

Applying the Laplace transform to (5)-(6) and using (10) leads to

$$pS_{f_0} r^{-b} \bar{H}_f(r,p) = \frac{K_{f_0}}{r} \frac{\partial}{\partial r}\left[r^{1-a} \frac{\partial \bar{H}_f(r,p)}{\partial r} \right] + \alpha_0 r^{-b} \left[\bar{H}_m(r,p) - \bar{H}_f(r,p) \right] \tag{12}$$

$$pS_{m_0} \bar{H}_m(r,p) = \alpha_0 \left[\bar{H}_f(r,p) - \bar{H}_m(r,p) \right] \tag{13}$$

Equation (13) can be rearranged

$$\bar{H}_m(r,p)=\frac{\alpha_0/S_{m_0}}{p+\alpha_0/S_{m_0}}\bar{H}_f(r,p) \tag{14}$$

Substituting (14) into (12) yields

$$r^2\frac{\partial^2\bar{H}_f}{\partial r^2}+(1-a)r\frac{\partial\bar{H}_f}{\partial r}-\frac{S_{f_0}}{K_{f_0}}\left[p+\frac{(\alpha_0/S_{f_0})p}{p+\alpha_0/S_{m_0}}\right]r^{a-b+2}\bar{H}_f=0 \tag{15}$$

Equation (15) is a second order ordinary differential equation; its general solution is of the form (cf. Polyanin and Zaitsev [22], page 159, equation (127))

$$\bar{H}_f(r,p)=r^{\frac{a}{2}}\left\{C_1J_\nu\left[\frac{2iS_{f_0}^{1/2}r^{n/2}}{nK_{f_0}^{1/2}}\sqrt{\mathrm{A}(p)}\right]+C_2Y_\nu\left[\frac{2iS_{f_0}^{1/2}r^{n/2}}{nK_{f_0}^{1/2}}\sqrt{\mathrm{A}(p)}\right]\right\} \tag{16}$$

where $n=a-b+2$, $\nu=\frac{a}{n}$, $\mathrm{A}(p)=p+\frac{(\alpha_0/S_{f_0})p}{p+\alpha_0/S_{m_0}}$, $J_\nu(z)$ and $Y_\nu(z)$ are the Bessel functions of the first and second kinds, respectively. The parameters C_1 and C_2 are constant that can be calculated using boundary conditions.

In the Laplace domain, the boundary conditions become

$$\lim_{r\to\infty}\bar{H}_f(r,p)=0 \tag{17}$$

and

$$\lim_{r\to 0}\left[-2\pi\mathrm{B}K_{f_0}r^{1-a}\frac{\partial\bar{H}_f(r,p)}{\partial r}\right]=\frac{Q_0}{p} \tag{18}$$

The solution of (15), taking into account the boundary conditions (17) and (18) is

$$\bar{H}_f(r,p)=\frac{2r^{\frac{a}{2}}}{n^{1-\nu}\pi\Gamma(1-\nu)\mathrm{B}K_{f_0}^{1-\nu/2}S_{f_0}^{\nu/2}}\frac{\bar{Q}(p)K_\nu\left[\frac{2S_{f_0}^{1/2}r^{n/2}}{nK_{f_0}^{1/2}}\sqrt{p+\frac{(\alpha_0/S_{f_0})p}{p+\alpha_0/S_{m_0}}}\right]}{\left[\sqrt{p+\frac{(\alpha_0/S_{f_0})p}{p+\alpha_0/S_{m_0}}}\right]^\nu} \tag{19}$$

where K_ν is the modified Bessel function of the second kind of order ν. More details about the derivation of the solution (19) are given in the Appendix.

3.2 Analytical solution in the time domain

The solution in the time domain $H_f(r,t)$ is sought using the convolution theorem of the Laplace transform [23]

$$L\left[\int_0^t y(\tau,t-\tau)\,\mathrm{d}\tau;t\to p\right]=L\left\{L\left[y(t_1,t_2);t_2\to p\right];t_1\to p\right\} \tag{20}$$

Hence, equation (19) is written as

$$\bar{H}_f(r,p)=\bar{H}_f(r;p_1,p_2)=\frac{2Q_0 r^{\frac{a}{2}}}{n^{1-\nu}\pi\Gamma(1-\nu)\mathrm{B}K_{f_0}^{1-\nu/2}S_{f_0}^{\nu/2}}\frac{K_\nu\left[\dfrac{2S_{f_0}^{1/2}r^{n/2}}{nK_{f_0}^{1/2}}\sqrt{p_1+\dfrac{(\alpha_0/S_{f_0})p_2}{p_2+\alpha_0/S_{m_0}}}\right]}{p_2\left[\sqrt{p_1+\dfrac{(\alpha_0/S_{f_0})p_2}{p_2+\alpha_0/S_{m_0}}}\right]^\nu} \tag{21}$$

where $p_1=p_2=p$ but different indexes are used to indicate that the inverse transformation is performed in two steps.

The different indexes used in (21) indicate that the inverse Laplace transform is developed in two steps. In a first step, the inverse Laplace transform with respect to the variable p_1 is expressed as follows

$$L^{-1}\left[\bar{H}_f(r;p_1,p_2);p_1\to t_1\right]=\frac{n^\nu Q_0 e^{-\frac{S_{f_0}r^n}{2n^2K_{f_0}t_1}}\cdot W_{\frac{1-\nu}{2},\frac{\nu}{2}}\left(\dfrac{S_{f_0}r^n}{n^2K_{f_0}t_1}\right)}{\pi\Gamma(1-\nu)\mathrm{B}K_{f_0}^{\frac{1-\nu}{2}}S_{f_0}^{\frac{1+\nu}{2}}r^{\frac{2-b}{2}}}\cdot\frac{e^{-\frac{(\alpha_0/S_{f_0})t_1p_2}{p_2+\alpha_0/S_{m_0}}}}{p_2} \tag{22}$$

where t_1 is the time variable obtained by the inverse Laplace transform with respect to the variable p_1 and $W_{\kappa,\mu}(z)$ is the Whittaker function (Abramowitz and Stegun [24] p. 505).

In the second step, the inverse Laplace transform with respect to p_2 is obtained using the inverse transform of the *J*-function [25] based on the formula $L^{-1}\left[\frac{1}{p}e^{-\frac{\alpha p}{p+\beta}};p\to t\right]=J\left(\alpha,\beta t\right)$ which yields

$$\bar{H}_f\left(r;p_1,p_2\right)=\frac{n^{\nu}Q_0e^{-\frac{S_{f_0}r^n}{2n^2K_{f_0}t_1}}\cdot t_1^{\frac{\nu-1}{2}}\cdot W_{\frac{1-\nu}{2},\frac{\nu}{2}}\left(\frac{S_{f_0}r^n}{n^2K_{f_0}t_1}\right)\cdot J\left(\frac{\alpha_0t_1}{S_{f_0}},\frac{\alpha_0t_2}{S_{m_0}}\right)}{2\pi\Gamma\left(1-\nu\right)\mathrm{B}K_{f_0}^{\frac{1-\nu}{2}}S_{f_0}^{\frac{1+\nu}{2}}r^{\frac{2-b}{2}}} \tag{23}$$

The Bessel integral *J*-function is defined as follows [8, 26]

$$J\left(a,b\right)=1-e^{-b}\int_0^a e^{-\lambda}I_0\left(2\sqrt{b\lambda}\right)\mathrm{d}\lambda=e^{-a-b}\sum_{n=0}^{\infty}\frac{b^n}{n!}\sum_{m=0}^{n}\frac{a^m}{m!} \tag{24}$$

In view of (20) and (23), the analytical expression of $H_f\left(r,t\right)$ is

$$H_f\left(r,t\right)=\frac{n^{\nu}Q_0}{2\pi\Gamma\left(1-\nu\right)\mathrm{B}K_{f_0}^{\frac{1-\nu}{2}}S_{f_0}^{\frac{1+\nu}{2}}r^{\frac{2-b}{2}}}\int_0^t\tau^{\frac{\nu-1}{2}}\cdot e^{-\frac{S_{f_0}r^n}{2n^2K_{f_0}\tau}}\cdot W_{\frac{1-\nu}{2},\frac{\nu}{2}}\left(\frac{S_{f_0}r^n}{n^2K_{f_0}\tau}\right)\cdot J\left(\frac{\alpha_0\tau}{S_{f_0}},\frac{\alpha_0\left(t-\tau\right)}{S_{m_0}}\right)\mathrm{d}\tau \tag{25}$$

A similar expression can be obtained for $H_m\left(r,t\right)$ using the convolution theorem of the Laplace transform for equation (14) and using equation (19).

In the case of homogeneous media $\left(a=b=0\right)$, we have $W_{\frac{1}{2},0}\left(z\right)=z^{\frac{1}{2}}e^{-\frac{z}{2}}$ and (25) reduces to the De Smedt [8] solution:

$$H_f\left(r,t\right)=\frac{Q_0}{4\pi\mathrm{B}K_{f_0}}\int_0^t\tau^{-1}e^{-\frac{S_{f_0}r^2}{4K_{f_0}\tau}}\cdot J\left(\frac{\alpha_0\tau}{S_{f_0}},\frac{\alpha_0\left(t-\tau\right)}{S_{m_0}}\right)\mathrm{d}\tau \tag{26}$$

4 COMPARISON TO NUMERICAL SOLUTIONS

We numerically solve two interference pumping tests dealing with homogeneous and fractal dual media. For each test, the numerical solution is compared against the corresponding analytical solution using (25). The numerical solution of the system (5)-(10) is developed using the standard Finite Volume (FV) method. The domain of size $L = 10,000\,m$ is discretized using a uniform spatial discretization of size $\Delta r = 5$ m. A similar solution is obtained using a finer spatial discretization of size $\Delta r = 1$m which shows the weak sensitivity of the numerical solution to the spatial discretization. The duration of the simulation is 2×10^6 s. Three time step sizes are investigated with $\Delta t = 10^5$ s, $\Delta t = 5\times10^4$ s and $\Delta t = 10^4$ s. The pumping flow rate is $Q_0 = 5$ m^3/h. The initial head in the aquifer is $h_0 = 100$ m and the aquifer thickness is $B = 100$ m. The specific storage of the fractures and rock matrix are respectively $S_{f_0} = 5\times10^{-6}$ m^{-1} and $S_{m_0} = 10^{-4}$ m^{-1}. The hydraulic conductivity of the fractures is $K_{f_0} = 10^{-4}$ m/s and the rate of exchange between the matrix and the fractures is $\alpha_0 = 5\times10^{-11}$ m^{-1}s^{-1}.

Figure 1 depicts the drawdown in both the fracture and matrix at 10m and 100m. The drawdown in the fissure starts at early times because storage of the fissures is immediately effective at the start of the pumping test, while storage of the matrix needs much more time to become noticeable. A flattening of the drawdown curve in the fissure can be observed at intermediate pumping time which is typical for double-porosity behavior because of the transition from fracture to matrix water storage release.

The numerical FV solution is compared to the analytical solution (25) in the case of homogeneous $(a = b = 0)$ and fractal $(a = 0.6$ and $b = 0.4)$ dual media. The comparison is performed at two observation wells located respectively at distances $r_1 = 10$ m and $r_2 = 100$ m from the pumping well. Significant discrepancies can be observed between analytical and numerical

196 solutions when the latter is evaluated using a large time step size (Figure 2). The drawdown in
197 the case of fractal dual media is larger than in homogeneous dual media because of the reduc-
198 tion of the hydrodynamic parameters with the distance r from the pumping well. In fact, in
199 the case of fractal dual media, the permeability of the fractures is proportional to $r^{-0.6}$ where-
200 as the exchange rate and the specific storage of both the fractures and the matrix are propor-
201 tional to $r^{-0.4}$. Thereby, the discrepancy between analytical and numerical solutions (Figure
202 2) is more pronounced with dual fractal media than with homogeneous dual media. For both
203 homogeneous and fractal dual media, the numerical solution converges toward the analytical
204 solution (25) when the size of the time step decreases (Figure 2). Note that the reduction of
205 the permeability of the fractures with respect to the distance r is also responsible, via the
206 Whittaker function in equation (25), of the delay for the stabilisation of the solution in the
207 fractal case (Figure 2 b) compared to the homogeneous case (Figure 2a).

208 ## 5 BAYESIAN INVERSION OF A PUMPING TEST IN FRACTAL DUAL MEDIA

209 In practical applications, most of the hydraulic parameters cannot be measured directly and
210 should be estimated using an inversion procedure. In the case of fractal dual media, the inver-
211 sion can be challenging because of model equifinality, implying that different parameter com-
212 binations can fit the model responses to data. To assess the applicability of the fractal dual
213 porosity model, the identifiability of the parameters of the analytical solution (25) is assessed
214 using a synthetic interference pumping test with a set of noisy data. Parameter identification is
215 performed in a Bayesian framework where the prior knowledge about the parameters and the
216 observed data are merged to define the joint posterior probability distribution function (pdf) of
217 the parameters. In this work, the pdf is performed using the DREAM$_{(ZS)}$ software [16] based
218 on the Markov Chain Monte Carlo (MCMC) sampler. DREAM$_{(ZS)}$ generates random se-
219 quences of parameter sets that asymptotically converge toward the target joint posterior dis-

tribution [27]. Thus, if the number of runs is sufficiently high, the generated samples allows exploring the entire parameter space of the posterior distribution of the parameters and provides the pairwise parameter correlations and the uncertainty of model predictions.

The Bayes theorem states that the probability density function of the model parameters conditioned onto data can be expressed as:

$$p(\boldsymbol{\xi} \mid \boldsymbol{y}_{mes}) \propto p(\boldsymbol{y}_{mes} \mid \boldsymbol{\xi})\, p(\boldsymbol{\xi}), \tag{27}$$

where $p(\boldsymbol{\xi} \mid \boldsymbol{y}_{mes})$ is the likelihood function measuring how well the model fits the observations $\boldsymbol{y}_{mes}$, and $p(\boldsymbol{\xi})$ is the prior information about the parameter before the observations are made. In this work, a Gaussian distribution defines the likelihood function because the *observations* are simulated and corrupted with Gaussian errors. Hence, the parameter posterior distribution is expressed as:

$$p(\boldsymbol{\xi} \mid \boldsymbol{y}_{mes}) \propto \sigma_h^{-N_h}\, exp\left(-\frac{SS_h(\boldsymbol{\xi})}{2\sigma_h^2}\right), \tag{28}$$

where $SS_h(\boldsymbol{\xi})$, are the sums of the squared differences between the observed and modeled drawdowns. For instance, $SS_h(\boldsymbol{\xi}) = \sum_{k=1}^{Nh}\left(h_{mes}^{(k)} - h_{mod}^{(k)}(\boldsymbol{\xi})\right)^2$, which includes the observed $h_{mes}^{(k)}$ and predicted $h_{mod}^{(k)}$ drawdowns at time t_k for the number of observations N_h.

A synthetic pumping test is generated by running the analytical solution using the reference parameter values given in Table 1 for K_{f_0}, S_{f_0}, α_0, a and b. As in Fahs *et al.* [28], the storage coefficient in the matrix S_{m_0} is fixed in this study to be 10^{-4} m^{-1}.

Delay et al [7] showed that results of calibration improved when several drawdown curves at several locations are inverted at once. In the sequel, the analytical solution is run for a long period of 2×10^7 s to calculate the drawdown at four observation wells located respectively at $r_1 = 1$ m, $r_2 = 10$ m, $r_3 = 100$ m and $r_4 = 500$ m from the pumping well. Four datasets of 2000

values each (corresponding to the drawdown at the observation wells measured each 10^4 s) are used as target responses for model inversion.

Gaussian noise with a standard deviation of 0.01m and a mean of zero was added to the target responses. We assume that all hydraulic parameters have uniform prior distributions over the ranges given in Table 1. As recommended in Vrugt *et al.* [29], we consider that the posterior distribution is stationary if the Gelman and Ruban [30] criterion is less than 1.2 and that the chains are not autocorrelated.

The MCMC method was terminated after 15000 model runs. The convergence was reached at around 10000 model runs. Figure 3 shows the results of the identification based on the last 25% of individuals of the MCMC sampler (when the chains have converged). The "on-diagonal" plots in these figures display the inferred parameter distributions, whereas the "off-diagonal" plots represent the pairwise correlations in the MCMC sample. If the drawings are independent, non-sloping scatterplots should be observed. However, if a good value of a given parameter is conditioned by the value of another parameter, then their pairwise scatterplot should show a narrow sloping stripe. The results of Figure 3 show that the five parameters K_{f_0}, S_{f_0}, α_0, a and b are appropriately estimated; they have almost symmetric bell-shaped posterior distributions and have strongly narrowed their prior intervals. The scatter plots in this figure show a moderate correlation between the parameters a and b (a correlation factor of 0.61), a high correlation between the parameters S_{f_0} and b (a correlation factor of 0.79) and a very high correlation between the parameters K_{f_0} and a (a correlation factor of 0.98). The mean and 95% confidence intervals of the samples that adequately fit the model onto observations are reported in Table 2. From this table, we can see that the parameters K_{f_0}, a and b are well identified with respectively a mean value of 0.99×10^{-5} ms^{-1}, 0.299 and 0.2. These values are almost identical to the reference values of Table 1. The uncertainty on these

parameters is small since the 95% confidence intervals are respectively [0.9-1.1]×10^{-5} ms^{-1}, [0.28-0.32] and [0.17-0.23]. The parameters S_{f_0} and α_0 are less well identified. Indeed, although their mean values (respectively 5.03×10^{-5} m^{-1} and 3.06×10^{-11} $m^{-1}s^{-1}$) are very close to the reference values, their posterior uncertainty remains quite large since their confidence intervals are respectively [3.2-7.6]×10^{-5} m^{-1} and [2.1-4.5]×10^{-11} $m^{-1}s^{-1}$.

Finally note that the identification procedure does not converge if the storage coefficient in the matrix S_{m_0} is involved in the inversion procedure (not fixed). In that case, the identification of the six parameters K_{f_0}, S_{f_0}, S_{m_0}, α_0, a and b was not possible. Indeed, in this case, the MCMC algorithm was faced to convergence problem because of equifinality issues.

6 CONCLUSION

A new analytical solution for interference hydraulic pumping tests in fractal fractured porous media is developed using the dual-porosity concept and power laws in space for all hydrodynamic parameters. The developed analytical solution is compared to a numerical one obtained with the FV method using different time step sizes. Discrepancies are observed between analytical and numerical solutions when the latter is used with large time steps. These discrepancies are more pronounced with dual fractal media than with homogeneous dual media. When the size of the time step decreases, the numerical solution converges toward the analytical one for both homogeneous and fractal dual media.

The applicability of the fractal dual-porosity model was then assessed by investigating identifiability of the hydraulic parameters from a synthetic interference pumping test with a set of noisy data using the MCMC sampler. The results show that if the storage coefficient in the

matrix is fixed, the rest of the parameters can be appropriately identified, whereas convergence problems can be encountered if all the hydraulic parameters are to be estimated.

Acknowledgements

This work was partially supported by the GdR MoMaS (PACEN/CNRS, ANDRA, BRGM, CEA, EDF, IRSN) France and by the French National Research Agency (ANR) through the program AAP Blanc - SIMI 6 project RESAIN (n◦ANR-12-BS06-0010-02).

Appendix: Derivation of the Analytical Solution in the Laplace Domain

Using the boundary condition at infinity (17) and the following asymptotic expansions for large arguments $\left(|z|\to\infty\right)$ of J_ν and Y_ν [22], $J_\nu(z)=\sqrt{2/\pi z}\left\{P(\nu,z)\cos\chi-Q(\nu,z)\sin\chi\right\}$ and $Y_\nu(z)=\sqrt{2/\pi z}\left\{P(\nu,z)\cos\chi+Q(\nu,z)\sin\chi\right\}$ for $|\arg z|<\pi$ with $\chi=z-\left(\frac{1}{2}\nu+\frac{1}{4}\right)\pi$, $P(\nu,z)=\sum_{k=0}^{\infty}(-1)^k\frac{(\nu,2k)}{(2z)^{2k}}$ and $Q(\nu,z)=\sum_{k=0}^{\infty}(-1)^k\frac{(\nu,2k+1)}{(2z)^{2k+1}}$, equation (16) gives $C_1+iC_2=0$. Therefore, this latter can be written as

$$\bar{H}_f(r,p)=C_1 r^{\frac{a}{2}}H_\nu^{(1)}\left[\frac{2iS_{f_0}^{1/2}r^{n/2}}{nK_{f_0}^{1/2}}\sqrt{\mathrm{A}(p)}\right] \tag{A.1}$$

where $H_\nu^{(1)}$ is the Hankel function of the first kind defined by $H_\nu^{(1)}(z)=J_\nu(z)+iY_\nu(z)$ for any complex number z.

The boundary condition at the well (18) is then used to find C_1. Note that for $\nu>0$ the Hankel function $H_\nu^{(1)}\sim-\frac{i}{\pi}\Gamma(\nu)\left(\frac{1}{2}z\right)^{-\nu}$ as z approaches zero [22], where Γ is the Gamma function. Using this expansion we can write

$$r^{1-a}\frac{\partial\bar{H}_f(r,t)}{\partial r}\sim\frac{i^{1-\nu}S_{f_0}^{\nu/2}C_1}{2\pi K_{f_0}^{\nu/2}}\left\{-r^{-a}n^\nu\left[\sqrt{A(p)}\right]^{-\nu}\left\{a\Gamma(\nu)-n\Gamma(1+\nu)\right\}+n^{1-\nu}\left[\sqrt{A(p)}\right]^{\nu}\Gamma(1-\nu)\right\} \tag{A.2}$$

312 as r appraches zero. Using the property of the Gamma function $\Gamma(1+\nu)=\nu\Gamma(\nu)$ for $\nu>0$,

313 the first term of right hand side of equation (A.2) vanishes since $n\nu=a$. Substituting (A.2)

314 into (18) we get $C_1=-\dfrac{\bar{Q}(p)}{i^{1-\nu}n^{1-\nu}\Gamma(1-\nu)\mathrm{B}K_{f_0}^{1-\nu/2}S_{f_0}^{\nu/2}\left[\sqrt{A(p)}\right]^{\nu}}$.

315 Finally, inserting the value of C_1 into (A.1) and using the relationship

316 $K_\nu(z)=\dfrac{1}{2}\pi i e^{\frac{1}{2}\nu\pi i}H_\nu^{(1)}\left(ze^{\frac{1}{2}\pi i}\right)$ for $-\pi<\arg z\le\dfrac{1}{2}\pi$, where K_ν is the modified Bessel func-

317 tion of the second kind of order ν, we get the solution in the Laplace domain as defined by

318 (19).

319

REFERENCES

[1] Hsieh, P.A.: A brief survey of hydraulic tests in fractured rocks. In Faybishenko B, Witherspoon PA, Benson SM (eds.) Dynamics of fluids in fractured rocks, American Geophysical Union Geophysical Monograph 122:59–66 (2000).

[2] Kruseman, G.P., de Ridder, N.A.: Analysis and evaluation of pumping test data. International Institute for Land Reclamation and Improvement Publication, Wageningen (1991).

[3] Batu, V.: Aquifer Hydraulics: a comprehensive guide to hydrogeologic data analysis. John Wiley & Sons Inc. New York (1998).

[4] Cheng, A.H.D.: Multilayered aquifer systems fundamentals and applications. Marcel Dekker, New York/Basel (2000).

[5] Walton, W.C.: Aquifer test modelling. CRC press, Taylor & Francis Group, Boca Raton (2006).

[6] Nielsen, K.A.: Fractured aquifers formation evaluation by Well Testing. Trafford Publishing, Canada (2007).

[7] Delay, F., Kaczmaryk, A., Ackerer, P.: Inversion of interference hydraulic pumping tests in both homogeneous and fractal dual media. Adv. in Water Resour. 30(3):314-334. (2007) doi:10.1016/j.advwatres.2006.06.008

[8] De Smedt, F.: Analytical solution Analytical Solution for Constant-Rate Pumping Test in Fissured Porous Media with Double-Porosity Behaviour. Transp Porous Med. 88:479-489 (2011). doi:10.1007/s11242-011-9750-9.

[9] Barenblatt ,G.E., Zheltov, I.P., Kochina, I.N.: Basis concepts in the theory of seepage of homogeneous liquids in fissured rocks. J. Appl. Math. Mech. Engl. Transl. 24(5):1286–1303 (1960). doi:10.1016/0021-8928(60)90107-6.

[10] Zhan, H., Wen, Z., Gao, G.: An analytical solution of two-dimensional reactive solute transport in an aquifer aquitard system. Water Resour. Res. 45, W10501. (2009). doi:10.1029/2008WR007479

[11] O'Shaughnessy, B., Procaccia, I.: Diffusion in fractals. Phys Rev A. ;32:3073 (1985) doi:10.1103/PhysRevA.32.3073

[12] Acuna, J.A., Yortsos, Y.C.: Application of fractal geometry to the study of networks of fractures and their pressure transient. Water Resour Res; 31(3):527–40 (1995). doi: 10.1029/94WR02260

[13] Chang, J., Yortsos, Y.C.: Pressure-transient analysis of fractal reservoirs. Soc Petrol Eng J 18710:631–43 (1990) doi:10.2118/18170-PA.

[14] Delay, F., Porel, G., Bernard, S.: Analytical 2D model to invert hydraulic pumping tests in fractured rocks with fractal behavior. Geophys Res Lett. 31(16) (2004). doi:10.1029/2004GL020500.

[15] Le Borgne, T., Bour, O., de Dreuzy, J.R., Davy, P., Touchard, F.: Equivalent mean flow models for fractured aquifers: insights for a pumping test scaling interpretation. Water Resour Res;40(3) (2004). doi:10.1029/2003WR002436.

[16] Laloy, E., Vrugt, J.A.: High-dimensional posterior exploration of hydrologic models using multiple-try DREAM(ZS) and high-performance computing, Water Resour. Res., 48 W01526. (2012). doi:10.1029/2011WR010608.

[17] Campbell, K.: Statistical calibration of computer simulations, Reliability Engineering and System Safety 91 1358–1363 (2006). doi:10.1016/j.ress.2005.11.032

[18] Warren, J.E., Root, P.J.: The behavior of naturally fractured reservoirs. Soc Petrol Eng 3:245–55. (1963). doi:10.2118/426-PA.

[19] Moench, A.F.: Double-porosity models for a fissured groundwater reservoir with fracture skin. Water Resour. Res. 20(7):831–846. (1984). doi:10.1029/WR020i007p00831.

[20] Chang, J., Yortsos, Y. C. A Note On Pressure-Transient Analysis Of Fractal Reservoirs. Society of Petroleum Engineers. (1993). doi:10.2118/25296-PA

372 [21] Hamm, S.Y., Bidaux, P. Dual-porosity fractal models for transient flow analysis in fis-
373 sured rocks: Water Resources Research, v. 32, no. 9, p. 2733-2745 (1996).

374 [22] Polyanin, A.D., Zaitsev, V.F. Handbook of Exact Solutions for Ordinary Differential
375 Equations, 2nd ed., 787 pp., Chapman and Hall/ CRC, Boca Raton, Fla (2003).

376 [23] Sneddon, I.H.: The Use of Integral Transforms, McGraw-Hill, New York (1972).

377 [24] Abramowitz, M., Stegun, I.A. Handbook of Mathematical Functions With Formulas,
378 Graphs, and Mathematical Tables, Government Printing Off., Washington, D. C.
379 (1972).

380 [25] Goldstein, F.R.S.: On the mathematics of exchange processes in fixed columns I: Math-
381 ematical solutions and asymptotic expansions. Proc. R. Soc. London 219: 151-185.
382 (1953).

383 [26] De Smedt, F., Wierenga, P.J.: A generalized solution for solute flow in soils with mobile
384 and immobile water. Water Resour. Res. 15(5): 1137-1141. (1979). doi:
385 10.1029/WR015i005p01137.

386 [27] Gelman, A., Carlin, J.B., Stren, H.S., Rubin, D.B. Bayesian data analysis (1997), Chap-
387 mann and Hall, London.

388 [28] Fahs, H., Hayek, M., Fahs, M., Younes, A.: An efficient numerical model for hydrody-
389 namic parameterization in 2D fractured dual-porosity media. Adv. Water Resour. 63:
390 179-193. (2013). doi: 10.1016/j.advwatres.2013.11.008

391 [29] Vrugt, J.A., Gupta, H.V., Bouten, W., Sorooshian, S. A shuffled complex evolution Me-
392 tropolis algorithm for optimization and uncertainty assessment for hydrologic model pa-
393 rameters. Water Resour. Res. 39(8):1201 (2003), doi:10.1029/2002WR001642.

394 [30] Gelman, A., Rubin, D.B. Inference from iterative simulation using multiple sequences.
395 Stat. Sci. 7:457-472 (1992). doi: 10.1214/ss/1177011136
396

List of Tables

List of Figures

Table 1

Parameters	Lower bounds	Upper bounds	Reference values
K_{f_0} [ms^{-1}]	5×10^{-7}	5×10^{-4}	1×10^{-5}
S_{f_0} [m^{-1}]	10^{-6}	10^{-3}	5×10^{-5}
α_0 [m^{-1}s^{-1}]	10^{-12}	10^{-9}	3×10^{-11}
a [-]	0.1	0.5	0.3
b [-]	0.1	0.5	0.2

Table 2

Parameters	Mean	95% Conf. Int.
K_{f_0} [ms^{-1}]	0.99×10^{-5}	$[0.9\text{-}1.1]\times10^{-5}$
S_{f_0} [m^{-1}]	5.03×10^{-5}	$[3.2\text{-}7.6]\times10^{-5}$
α_0 [m^{-1}s^{-1}]	3.06×10^{-11}	$[2.1\text{-}4.5]\times10^{-11}$
a [-]	0.299	[0.28-0.32]
b [-]	0.2	[0.17-0.23]

442 **Figure 1**

443

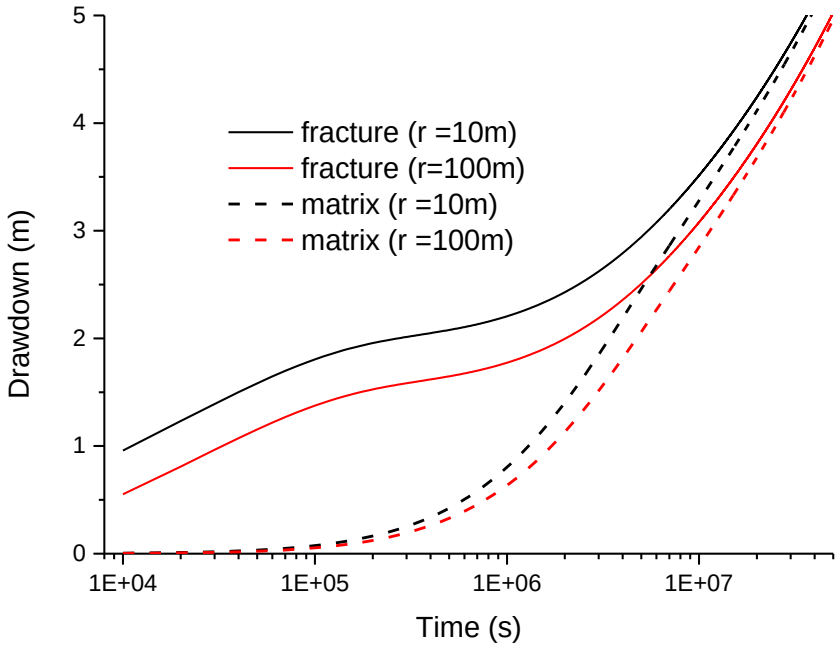

444

445

446

447 **Figure 2**

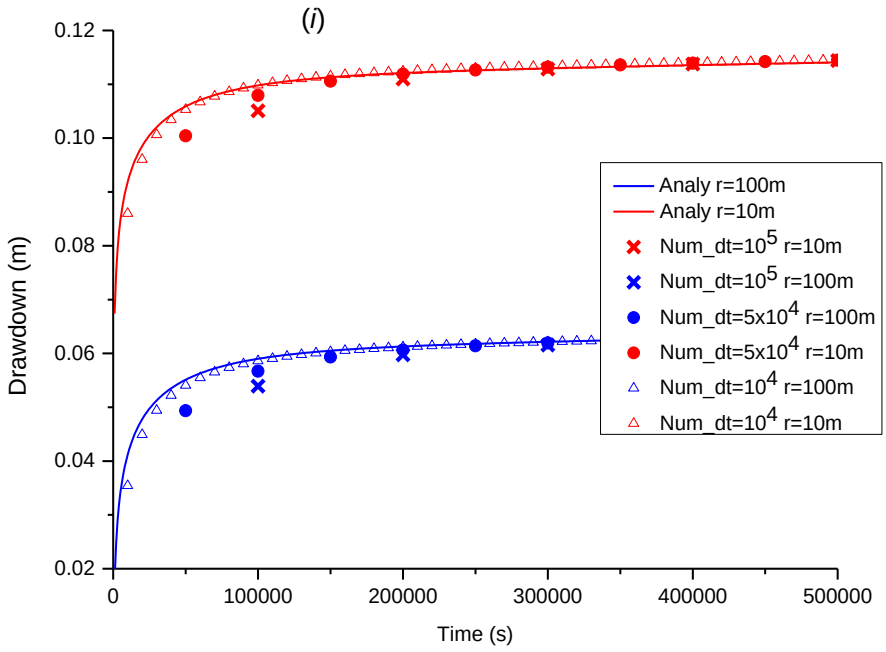

448

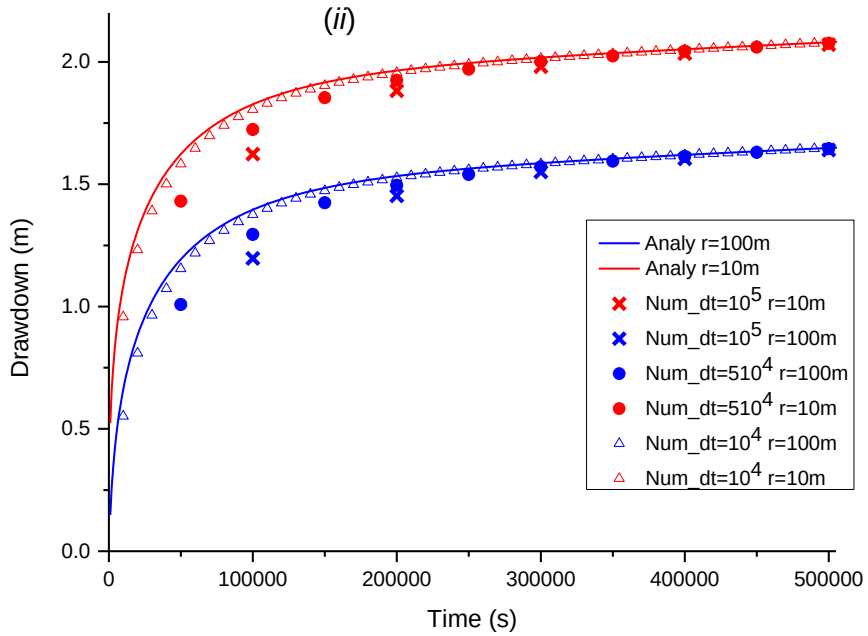

449

450

Figure 3

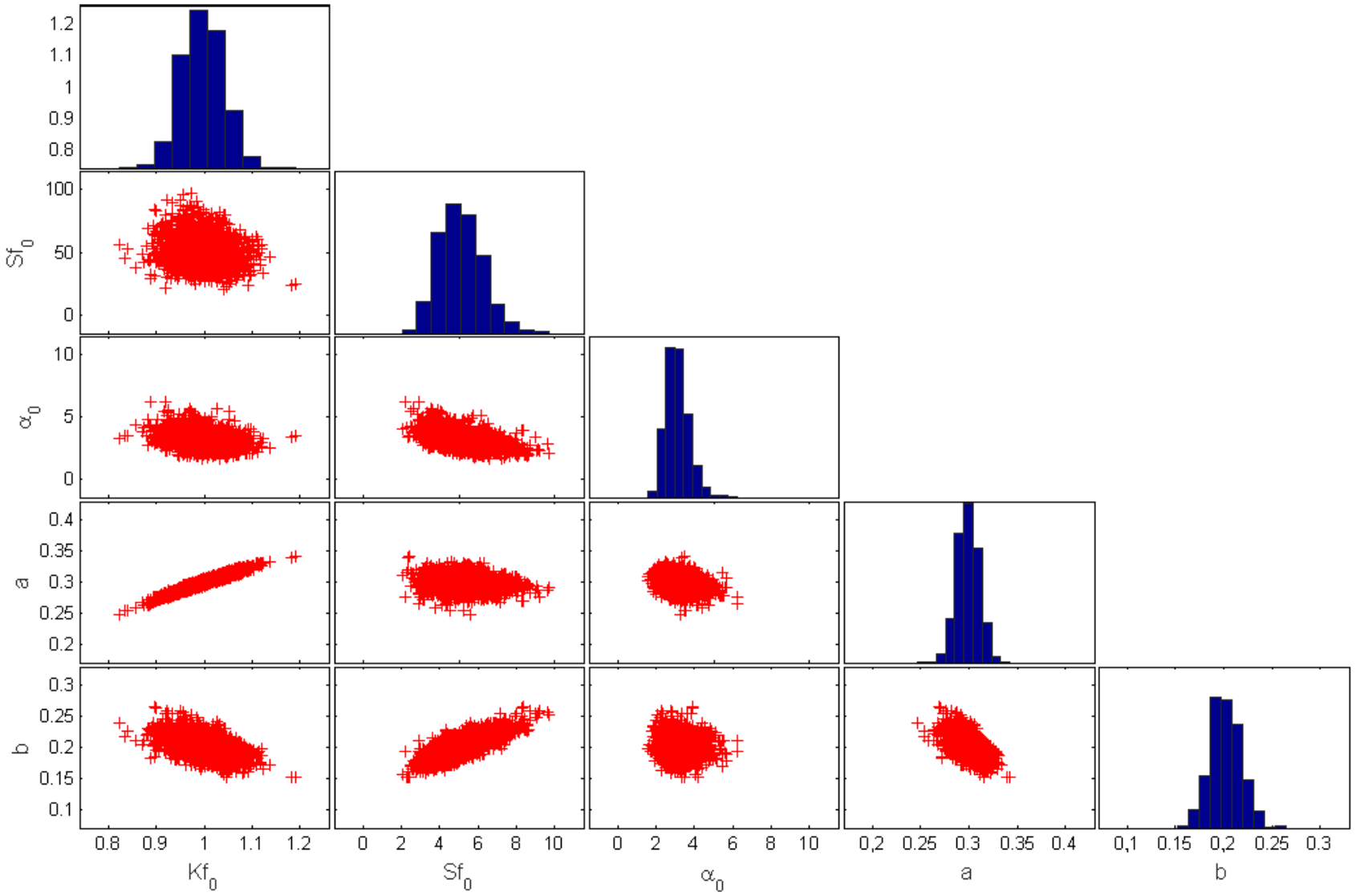
1.2
1.1
1
0.9
0.8
100
50
0
Sf_0
10
5
0
α_0
0.4
0.35
0.3
0.25
0.2
a
0.3
0.25
0.2
0.15
0.1
b
0.8 0.9 1 1.1 1.2
Kf_0
0 2 4 6 8 10
Sf_0
0 2 4 6 8 10
α_0
0,2 0.25 0.3 0.35 0.4
a
0,1 0.15 0,2 0.25 0.3
b